A Sacrificial 3D Printed Vessel-on-Chip Demonstrates a Versatile Approach to Model Connective Tissue Pathology

*Jonas Jäger, Phil Berger, Andrew I. Morrison, Hendrik Erfurth, Maria Thon, Eva-Maria Dehne, Susan Gibbs, and Jasper J. Koning**

*correspondence: jj.koning@amsterdamumc.nl

J.J, A.I.M., M.T., J.J.K.

Amsterdam UMC location Vrije Universiteit Amsterdam, Department of Molecular Cell Biology and Immunology, De Boelelaan 1117, Amsterdam, The Netherlands

Amsterdam institute for Immunology and Infectious diseases, Inflammatory diseases, Amsterdam, The Netherlands

P.B., H.E., E.D.

TissUse GmbH, Berlin, Germany

S.G.

Amsterdam UMC location Vrije Universiteit Amsterdam, Department of Molecular Cell Biology and Immunology, De Boelelaan 1117, Amsterdam, The Netherlands

Amsterdam institute for Immunology and Infectious diseases, Inflammatory diseases, Amsterdam, The Netherlands

Department of Oral Cell Biology, Academic Centre for Dentistry Amsterdam (ACTA), University of Amsterdam and Vrije Universiteit, Amsterdam, The Netherlands

Keywords: Microfluidics; Tissue engineering; 3D printing; Vascularization; Immunology

ORCID iD

Jonas Jäger	0000-0001-5326-9933
Phil Berger	0009-0000-3526-4805
Andrew I. Morrison	0009-0000-4144-9195
Hendrik Erfurth	0000-0003-3548-4888
Maria Thon	0000-0003-2380-7846
Eva-Maria Dehne	0000-0001-5694-6549
Susan Gibbs	0000-0002-3446-6138
Jasper J. Koning	0000-0003-2243-4857

Abstract

For *in vitro* organ models, perfused vasculature is crucial to overcome nutrient diffusion limits and to generate immunocompetent models by allowing trans-endothelial migration of immune cells in and out of the tissue. However, vasculature is often disregarded due to its complexity to generate and the necessity to integrate flow. The aim here was to overcome these limitations by combining 3D printing and multi-organ-chip technology to generate a vascularized, fibroblast-populated connective tissue matrix on-chip. A 3D printed, sacrificial, water-dissolvable structure was incorporated into a multi-organ-chip during its fabrication and hollow channels within a collagen/fibrin hydrogel were generated. Subsequently, channels were populated with endothelial cells and varying hydrogel concentrations (F_{high}/C_{high}) used to mimic healthy and diseased connective tissue. The vessels were perfused and stable metabolic/viability conditions (lactate dehydrogenase, glucose, lactate) acquired after 3 days for at least 7 days. Angiogenic sprouting and secretion of angiogenic cytokines were increased in F_{high} hydrogels. Perfusion with monocytes revealed differentiation into macrophages and migration across the endothelium into the tissue. In conclusion, this versatile, easy method to pattern hydrogels in a multi-organ-chip can serve as the basis to build the next generation of vascularized, immunocompetent human organ models, and opens new possibilities to study health and disease.

1. Introduction

In the human body, all cells inhabit a three-dimensional (3D) tissue-specific niche. They are embedded in a network of acellular molecules called the extracellular matrix (ECM), which provides structural support and biochemical cues. Molecular composition is highly variable and can change with age, tissue damage (wounding leading to fibrosis) and disease (tumor).[1] To maintain homeostasis, cells embedded in the ECM require a consistent supply of oxygen, nutrients, and the removal of waste products. To facilitate this, the ECM is penetrated by the blood vasculature, which comprises a complex system of arteries, veins, and capillaries. Furthermore, systemic circulation enables communication across organs through factors such as soluble mediators, exosomes, or cells to maintain viability and homeostasis.[2, 3] The inner layer of blood vessels and capillaries is directly in contact with the circulating blood and consists of a single layer of endothelial cells (ECs), known as the endothelium. Maintaining its integrity, ECs are connected via tight junctions and adherens junctions, transmembrane proteins such as platelet endothelial cell adhesion molecule 1 (PECAM-1; also known as CD31) and vascular endothelial cadherin (VE-cadherin; also known as CD144) to form a barrier.[4] However, cell-cell junctions are not always tightly closed. At sites of infection or injury, coordinated opening leads to the extravasation of immune cells such as monocytes, neutrophils, or lymphocytes out of the blood into the surrounding tissue to elicit an immune response.[5] Predominantly but not exclusively during development, blood vessels are either formed by vasculogenesis, *de novo* from endothelial progenitors or by sprouting from pre-existing ones in a process known as angiogenesis.[6] Vascular sprouting is also common in the fibrin-rich granulation tissue that forms in wound beds. This can lead to the formation of scars (fibrosis).[7]

In recent years, the engineering of human three-dimensional (3D) *in vitro* models has improved significantly.[8] Advanced models can recapitulate human biology and create more physiologically relevant human organ and tissue models. Microphysiological systems (MPS) have emerged, which are models mimicking human tissue and organ function *in vitro* at the micrometer scale. A type of MPS are Organ-on-Chip (OoC) systems which allow continuous organ, organoid or tissue model perfusion with small fluid volumes.[9, 10] Whereas OoC systems incorporate (mostly) only one organ or tissue, multi-organ-chips (MOC) take the OoC concept further, emulating human complexity and allowing crosstalk between different organs. This enables drug testing and disease modelling on a systemic level, which is particularly important

when studying drug absorption, distribution, metabolism, and excretion (ADME) as well as modelling inflammation and immunological diseases.[3, 11]

Modeling perfused blood vasculature presents a challenge, as it comprises the combination of an OoC with ECs, ideally within an ECM to allow angiogenic sprouting and integration of other relevant cell types such as fibroblasts, pericytes and smooth muscle cells. Several perfused vascularized organ models have been generated already.[12-19] However, most of these models rely on gravity-driven or laminar, non-recirculating flow with soft tubing, which complicates multi-organ cultures. In addition, these studies utilize highly customized in-house fabricated chip setups, which are not commercially available and very challenging to reproduce. Furthermore, several barrier models of e.g., skin, gut and lung make use of a transwell system on which the epithelium is grown on the upper side of a porous membrane with perfusion on the lower side.[20-22] This configuration makes it almost impossible to generate a perfused vascular network within the barrier model.

Addressing these issues, the aim of this study was to generate and characterize a vascularized, perfused fibroblast-containing connective tissue hydrogel directly inside a MOC platform and, perfused with peripheral blood-derived human monocytes. As OoC platforms are required to mimic healthy and diseased tissues, the objective was to highlight the versatility of the platform by modifying the hydrogel composition. Both collagen and fibrinogen are widely used for constructing hydrogels in tissue engineering. However, fibrin is also involved in granulation tissue formation, blood clotting and the inflammatory response of early wound healing which eventually leads to fibrosis.[7, 23] Accordingly, two different hydrogels were compared: a high collagen (C_{high}) hydrogel to mimic a healthy situation and a high fibrinogen (F_{high}) hydrogel to mimic the onset of inflammation and early granulation tissue. The vessel within the hydrogel was perfused for up to 7 days, while metabolic markers and viability of the EC-fibroblast co-cultures were assessed throughout the experiment. Following perfusion of monocytes, the differentiation into macrophages and migration into the tissue was evaluated. Overall, perfusable blood vessels were generated on-chip and it was demonstrated that the hydrogel composition can be modified to mimic early granulation tissue.

2. Results

2.1. Manufacturing of the chip platform

The MOC HUMIMIC Chip2 24-well (TissUse, Berlin, Germany) was utilized and produced as described earlier.[24] In brief, a microscopic glass slide was attached to a PDMS layer incorporating a closed loop of microfluidic channels. The circulation can be accessed from the top by two cell culture compartments, one with a diameter of 6.5 mm (vascular compartment) and one with a diameter of 14 mm (hydrogel compartment). The PDMS layer was attached to a polycarbonate adapter plate on the upper side, which served as a housing for cell culture compartments, lids, and pump adapters (**Figure 1A**). To apply flow, the on-chip micropumps were actuated by connecting the pump adapters via tubing to a HUMIMIC Starter control unit (TissUse). A 3D-printed sacrificial polyvinyl alcohol (PVA) structure was printed outside of the chip, incorporated in the hydrogel compartment, and aligned with the on-chip circulation when plasma-bonding the glass slide to the PDMS layer (**Figure 1A**, Supplementary Figure S1C). The versatility of 3D printing allowed for multiple vascular designs to be printed. However, in this study, either a straight line or a bifurcated print was incorporated into the chips (**Figure 1B**, i and ii).

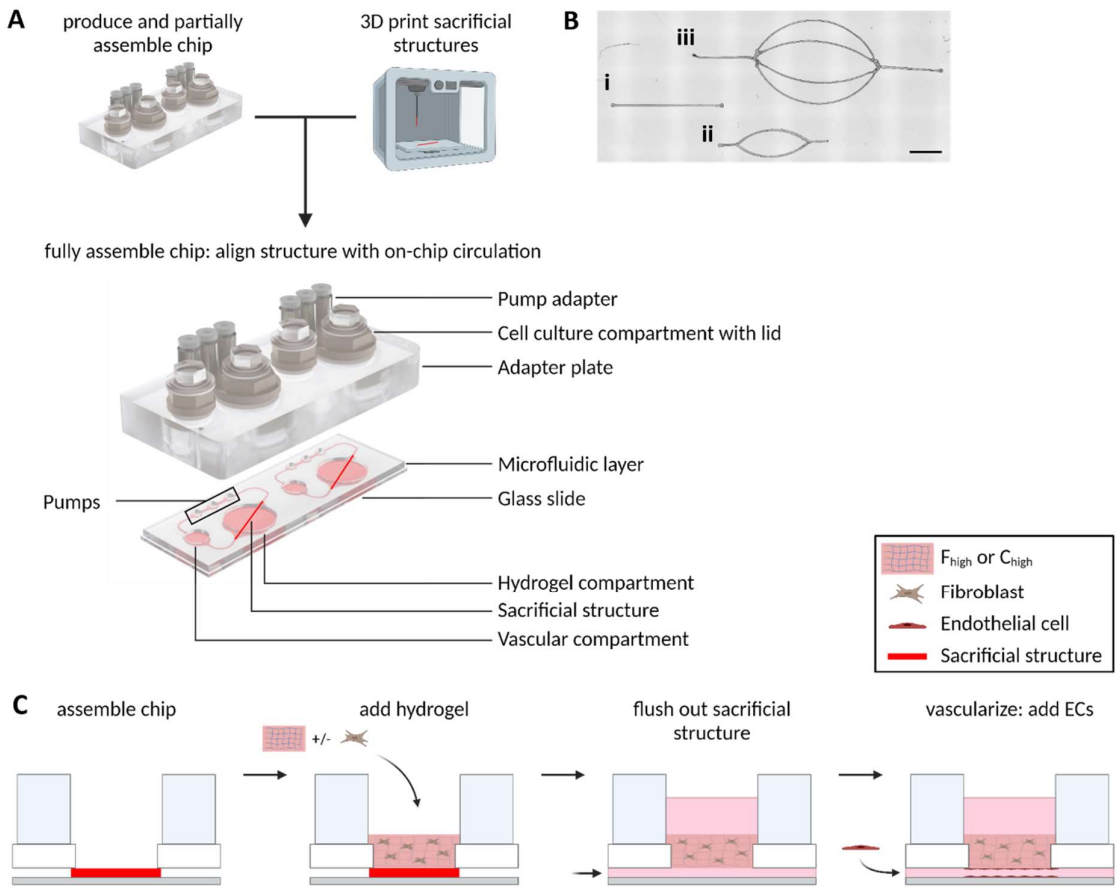

Figure 1: Sacrificial structure incorporated into the multi-organ-chip (MOC) platform to generate perfused vasculature. (A) Production of the chip by the integration of a 3D printed sacrificial structure in the MOC. The structure is incorporated in the hydrogel compartment and aligned with the on-chip circulation. One MOC consists of two independent circuits with a closed microfluidic loop. **(B)** 3D printing allows generation of different print designs. For simplification, design (i) and (ii) were used in this study. Scale bar: 3000 µm. **(C)** Cross-sectional view of the hydrogel compartment. Perfused vasculature is generated in three steps: addition of the hydrogel, removal of the sacrificial support structure and subsequent seeding of endothelial cells. F_{high}: high fibrinogen, C_{high}: high collagen hydrogel concentrations.

2.2. Hydrogel channel generation and characterization of flow profiles and shear stress

After manufacturing of the MOC, channels were generated within the hydrogel directly on the chip. Therefore, a hydrogel was layered on top of the sacrificial structure. While the PVA structure was dissolved, the hydrogel polymerized which resulted in a hollow channel within

the hydrogel, connected to the on-chip microcirculation (**Figure 1C**). Since it was unknown how the introduction of a hydrogel channel would change the flow within the chip, flow profiles and shear stress were first evaluated. Before the incorporation of cells, flow and shear stress in the hydrogel vessel were characterized and compared to the PDMS channel of chips without a hydrogel.

Notably, the chip without a hydrogel showed the typical pulsed flow profile with a short backflow followed by two peaks at a maximum flow rate of 76.8 µl/min (**Figure 2A**, top).[25] In contrast, the flow profile in the hydrogel vessel was clearly smoothened with no peaks and a more constant flow of 1.6 µl/min (**Figure 2A**, bottom). Addition of the hydrogel vessel decreased the average flow rate Q_{mean} from 7.0 to 2.2 µL/min and the extrema from 36.8 to 0.4 µL/min (**Figure 2B**, left). The mean wall shear stress (WSS) was reduced from 4.5 dyn/cm^2 to 0.04 dyn/cm^2 and extrema even further from 6.9 dyn/cm^2 to 0.01 dyn/cm^2 (**Figure 2B**, right). Computational fluid dynamics simulation shows highest velocity in the center of the cross section and highest shear stress in the center of top and bottom of the semi-elliptical channel walls, 7 times higher compared to the sides of the channel (**Figure 2C**).

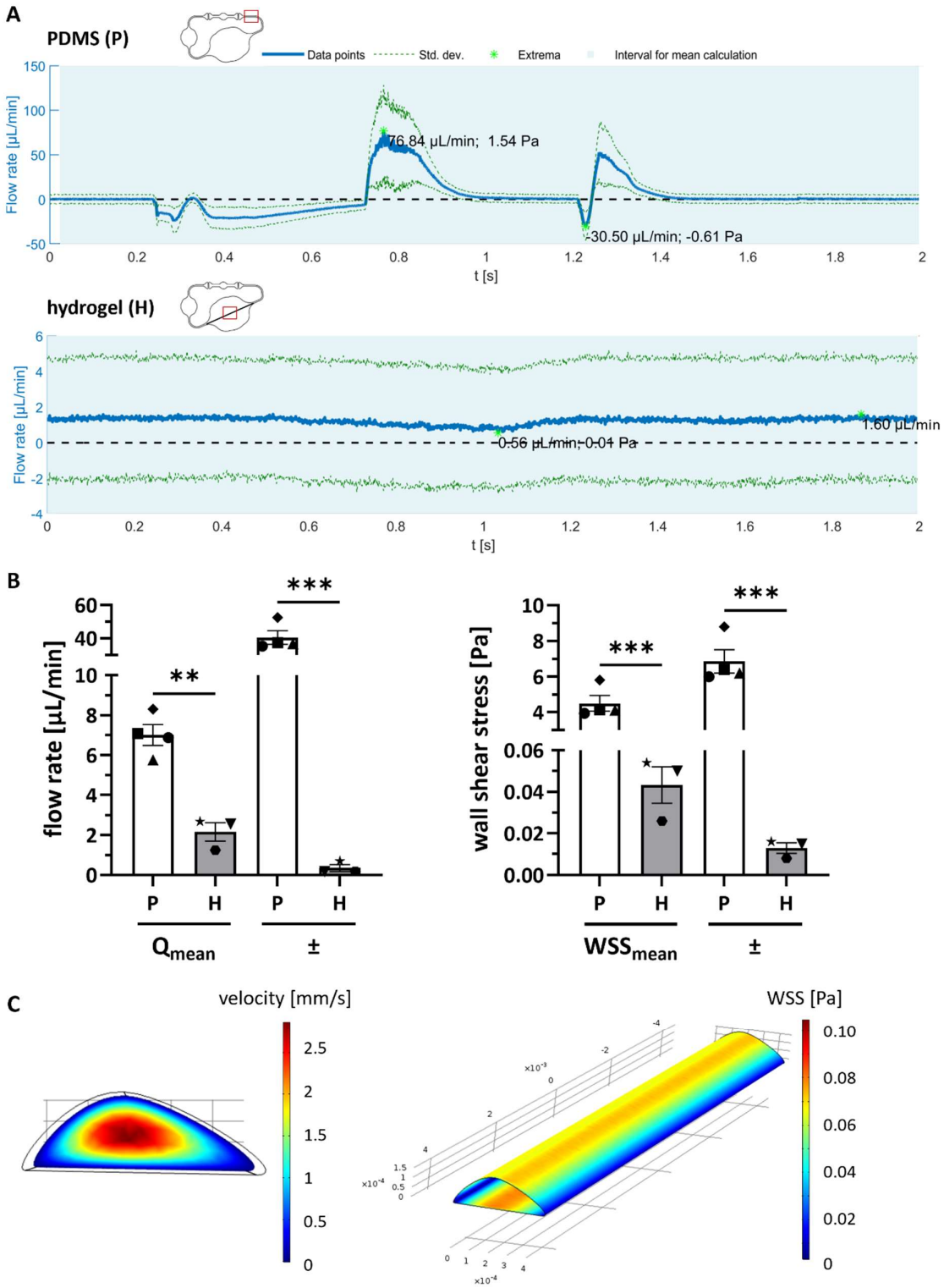

Figure 2: Hydrogel channel characterization: flow rate and shear stress. (A) Flow rate characterization in chips with and without print in different areas of the chip (as indicated with red squares), measured by non-invasive micro-particle image velocimetry. Representative flow

profiles are shown. Blue line represents data points and green dashed line standard deviation. **(B)** Quantified average flow rate (Q_{mean}) and mean wall shear stress (WSS_{mean}) with extrema (+/-) in respective areas as indicated in (A), P: PDMS, H: hydrogel. Mean ± SEM of n ≥ 3 individual microfluidic circuits are shown. **(C)** Simulated spatial resolution of velocity in the cross section and simulated WSS in a section of the hydrogel channel. PDMS: polydimethylsiloxane.

2.3. Generation of a functional vessel by endothelial cell population

After flow rate and shear stress characterization, a blood vessel was generated within the hydrogel (**Figure 1C**; for timeline, see Supplementary Figure S1B). Therefore, the hollow channels of a bifurcated sacrificial print were populated with ECs and the vessels cultured in flow for 7 days (**Figure 1B and 3A**). Notably, cells not only populated the entire channels (sides, top and bottom), but also aligned with shear stress in the direction of flow within the hydrogel vessel and the PDMS circulation (**Figure 3B**). A lumen was generated with a cross-section of semi-elliptical shape because of the negative mold of the print (**Figure 3C** and Supplementary Movie S1). To assess barrier properties of the generated vessel, a FITC-dextran permeability assay was performed. After 10 minutes, 70 kDa FITC-dextran was only detected strongly within the vessel, while no FITC-dextran was detected within the hydrogel. In contrast, channels without ECs showed clear diffusion of FITC-dextran into the hydrogel (**Figure 3D**). Overall, a functional vessel could be generated on-chip by population of the hydrogel channels with ECs.

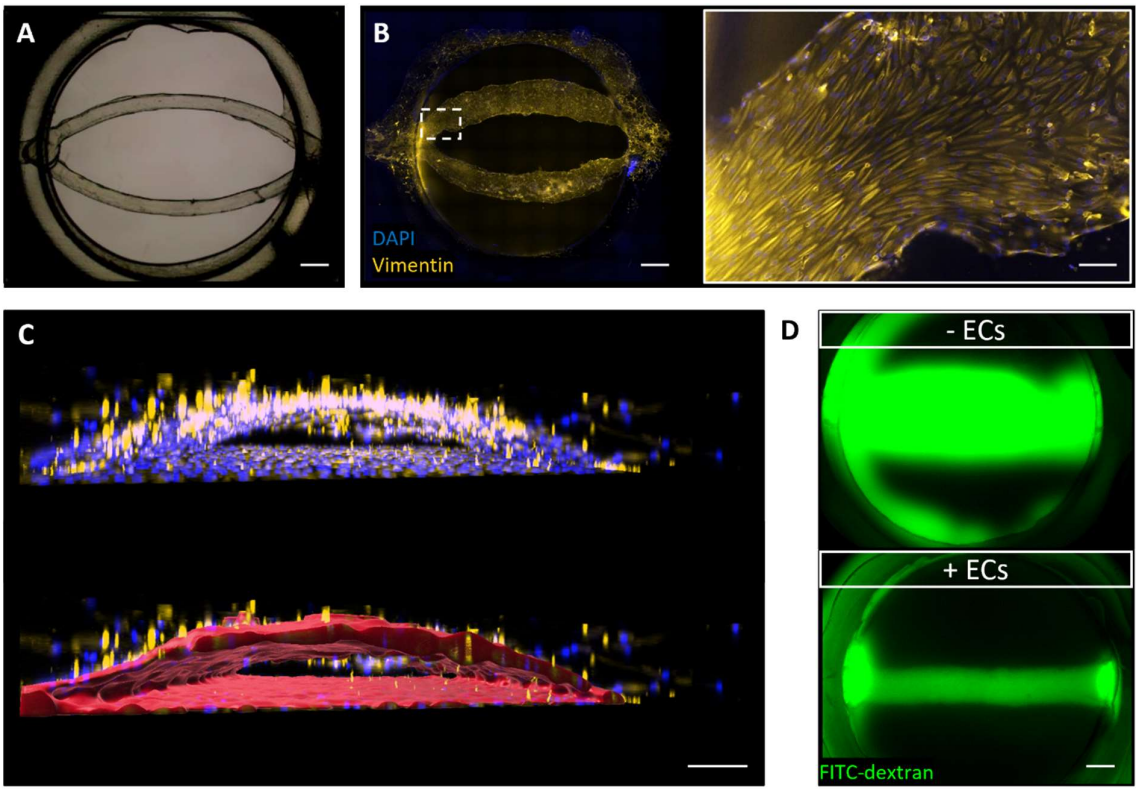

Figure 3: Endothelial cells grow on channel walls and form a functional, perfusable vessel on-chip. (A) Bright field image of a bifurcated sacrificial structure inside the hydrogel compartment. **(B)** Bottom view of the compartment on day 7. Endothelial cells (ECs) in chip populate the channel walls and align in direction of flow. **(C)** Surface rendering (red) visualizes hollow channels and semi-elliptical cross section. **(D)** FITC-dextran perfusion in channel with or without ECs shows perfusability and barrier properties of the blood vessel. ECs: Endothelial cells, FITC: Fluorescein isothiocyanate. PDMS: polydimethylsiloxane. Scale bars: 800 µm for overviews, 100 µm for magnification in (B) and 200 µm for magnifications in (C).

2.4. Hydrogel composition influences fibroblast and vessel morphology

Next, two hydrogel conditions were compared: high collagen (C_{high}) hydrogel to mimic the healthy state and high fibrinogen (F_{high}) hydrogel to model early granulation tissue. Additionally, fibroblasts were incorporated into the hydrogel to model the connective tissue.

Angiogenic sprouting was observed in the blood vessel in F_{high} but not in C_{high} hydrogels (**Figure 4A** and **B**, i). In addition, morphology of the fibroblasts changed noticeably from star-shaped in

F_{high} to elongated cells in C_{high} (**Figure 4B**, ii and iii). Channel width increased after addition of a hydrogel on top of the sacrificial structure, which had an initial width of 420 µm ± 3 µm after printing (**Figure 4C**). This widening was influenced by the composition of the hydrogel and much more pronounced in F_{high} hydrogels (605 µm ± 20 µm) than in C_{high} hydrogels (481 µm ± 6 µm). Compared to the condition without a hydrogel, the increase in channel width with cells was more pronounced in F_{high} (587 µm ± 17 µm with ECs only, 641 µm ± 32 µm with ECs and fibroblasts) compared to C_{high} (489 µm ± 14 µm with ECs only, 498 µm ± 25 µm with ECs and fibroblasts). **However**, the variability of the channel width also increased with the addition of ECs and fibroblasts. Overall, this further emphasizes the effect of the hydrogel composition and the ability of cells to influence the vessel morphology.

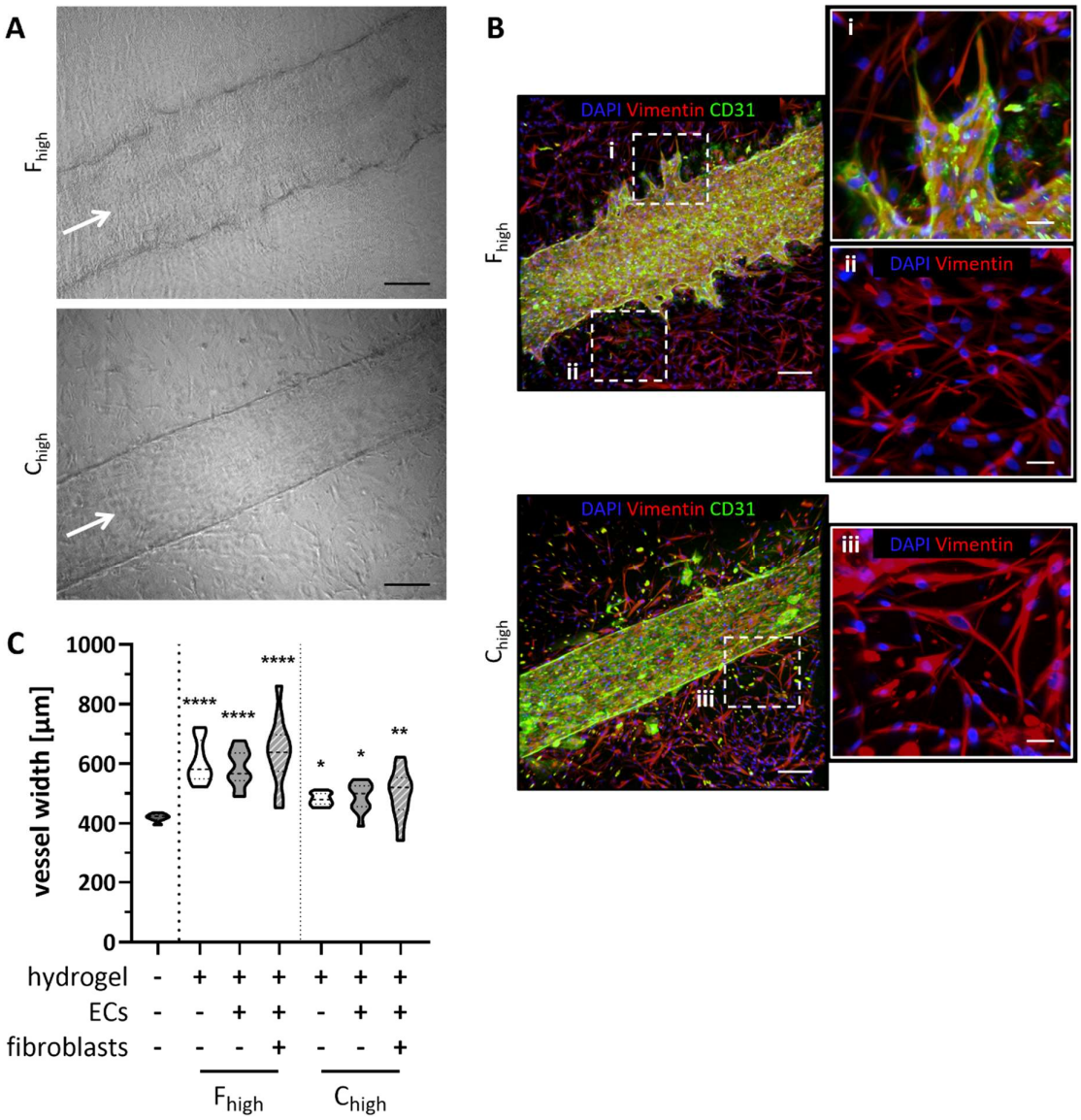

Figure 4: Hydrogel composition influences angiogenic sprouting, fibroblast morphology and channel width. (A) Vessel morphology changes with hydrogel composition. White arrows indicate the direction of perfusion. Scale bars: 200 µm. **(B)** Immunofluorescent staining reveals fibroblasts (vimentin, red) and ECs (CD31, green) in F_{high} and C_{high} hydrogels. Magnifications visualize angiogenic sprouting (i) and fibroblast morphology (ii, iii) within respective hydrogels. Maximum intensity projections are shown. Scale bars: 200 µm in overviews, 50 µm in magnifications. **(C)** Width of the vessel within the hydrogel is influenced by the hydrogel composition and presence of ECs and fibroblasts. The sacrificial print without a hydrogel was used as a control. Each condition contains $n \geq 10$ data points, which are compared to the control (-/-/-) with a one-way ANOVA. ****$p < 0.0001$, **$p \leq 0.01$, *$p \leq 0.05$.

2.5. Pro-inflammatory cytokine secretion increased in hydrogel medium and higher angiogenic cytokine secretion in F_{high} vessels

As angiogenic sprouting was observed into F_{high} but not into C_{high} hydrogels, secretion of angiogenic (bFGF, VEGF, sPECAM-1, EGF, angiopoeitin-1 and angiopoeitin-2) and pro-inflammatory cytokines (TNF-α, IL-6, IL-8) was investigated. The chip setup allowed for the separate sampling of culture supernatant from the vascular and from the hydrogel compartment (**Figure 1**). This enabled the comparison of cytokines within the circulation and on top of the hydrogel (**Figure 5A**). A trend of higher secretion in the hydrogel compared to the vasculature supernatant was detected for IL-6, IL-8 and angiopoietin-1 was detected at higher concentrations (**Figure 5B, C**). In contrast, bFGF and EGF were detected at higher levels in the vasculature supernatant (**Figure 5C**). The other proteins showed no significant difference in secretion between the two compartments. Notably, the presence or absence of fibroblasts in the hydrogel did not influence the secretion of any of the pro-inflammatory cytokines into the supernatant. However, when comparing F_{high} and C_{high} for angiogenic cytokine secretion, the angiogenic factors bFGF, VEGF and sPECAM-1 were secreted at higher levels into the vasculature in F_{high} conditions when fibroblasts were present in the hydrogel. sPECAM-1 was also secreted at higher levels in both vasculature and hydrogel, in the F_{high} compared to C_{high} condition. These results are all in line with the observed increase in angiogenic sprouting in F_{high} conditions (**Figure 5C**).

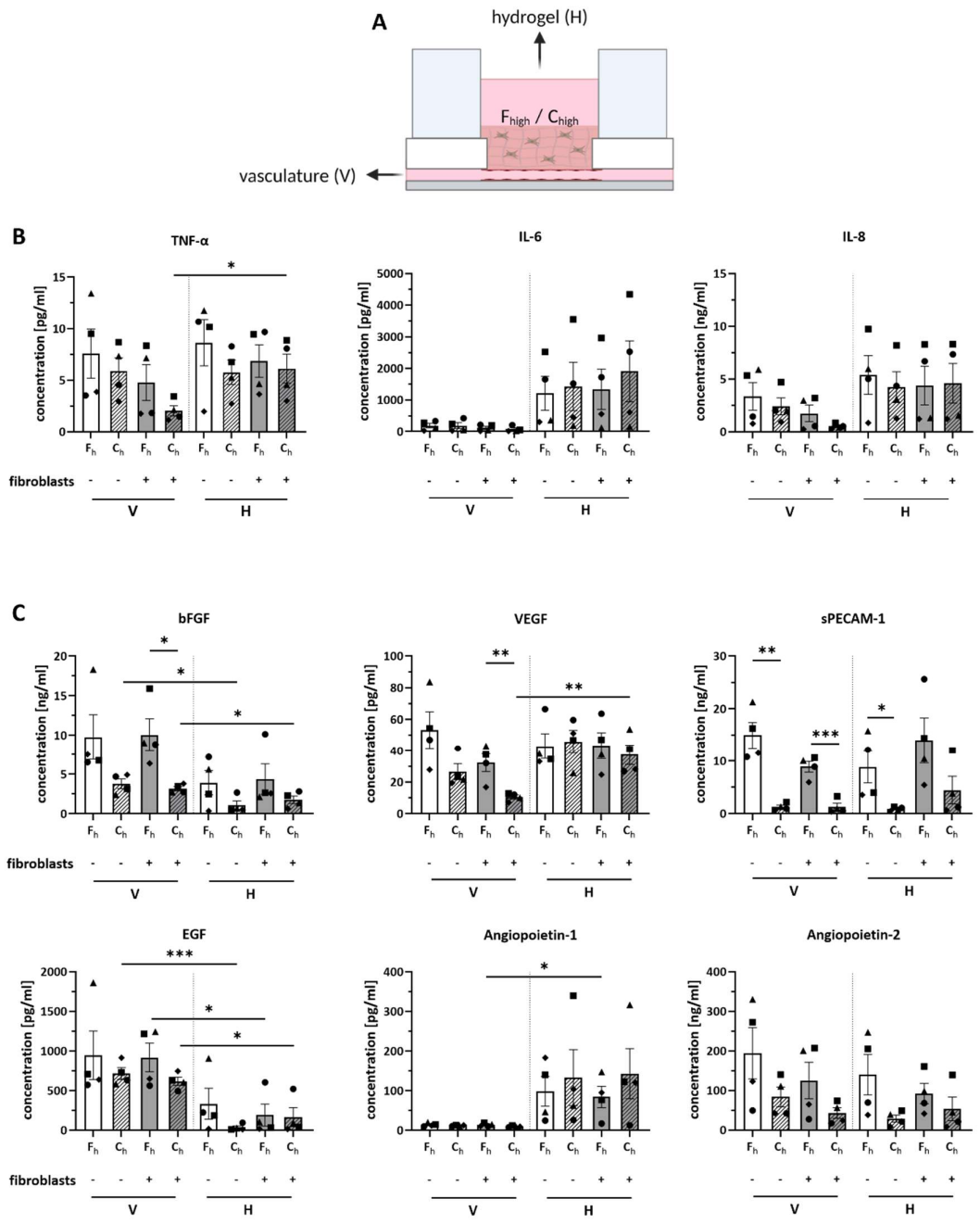

Figure 5: Elevated pro-inflammatory cytokine secretion in hydrogel medium and higher angiogenic cytokine secretion in F_{high} vasculature. (A) Medium was sampled either from the vasculature or the hydrogel on day 7. Hydrogel was added with or without fibroblasts in F_{high} and C_{high} hydrogels. **(B)** Pro-inflammatory cytokine and **(C)** Angiogenic cytokine concentrations. F_h: high fibrinogen, C_h: high collagen hydrogel concentrations; V: vasculature, H: hydrogel. Shapes represent different donors and columns mean ± SEM; n = 4 independent experiments

performed with a minimum of two intra-experimental replicates; ****$p \leq 0.0001$, ***$p \leq 0.001$, **$p \leq 0.01$, *$p \leq 0.05$, tested with unpaired t-test.

2.6. Vessel co-cultures in are metabolically stable and viable in chips for 7 days

To determine whether the F_{high} and C_{high} hydrogels with fibroblasts and ECs were metabolically active and viable in the chip, glucose, lactate and LDH concentrations were measured in the culture medium. We first assessed basal glucose levels of vasculature and hydrogel medium (indicated by dotted lines) and calculated glucose levels in the whole circulation (dashed line; **Figure 6**). In both the vasculature and hydrogel compartments, glucose consumption was higher when fibroblasts and ECs were present compared to ECs alone. Interestingly, glucose levels in the circulation were lower in F_{high} hydrogels when compared to C_{high} hydrogels (**Figure 6A**). In line with glucose measurements, lactate secretion was also higher when fibroblasts and ECs were present compared to EC alone. The highest secretion was observed in the F_{high} hydrogel with fibroblasts (**Figure 6B**). Glucose and lactate concentrations in the vasculature and on top of the hydrogel both increased from day 0 to 3 and then remained stable until day 7. LDH release, an indication for cell death and membrane porosity, reached its peak in all conditions at day 3 and then decreased from day 5 onwards (**Figure 6C**). Peaks were less pronounced in the hydrogel compared to the vasculature supernatant. Taken together, these results show that the metabolic biomarkers of glucose consumption and lactate secretion increased up to day 3 and stabilized over time until day 7. This coincides with LDH release which reached its maximum on day 3 and gradually decreased afterwards. Accordingly, a stable co-culture of ECs and fibroblasts is achieved in the chip after 3 days and remains stable until at least day 7.

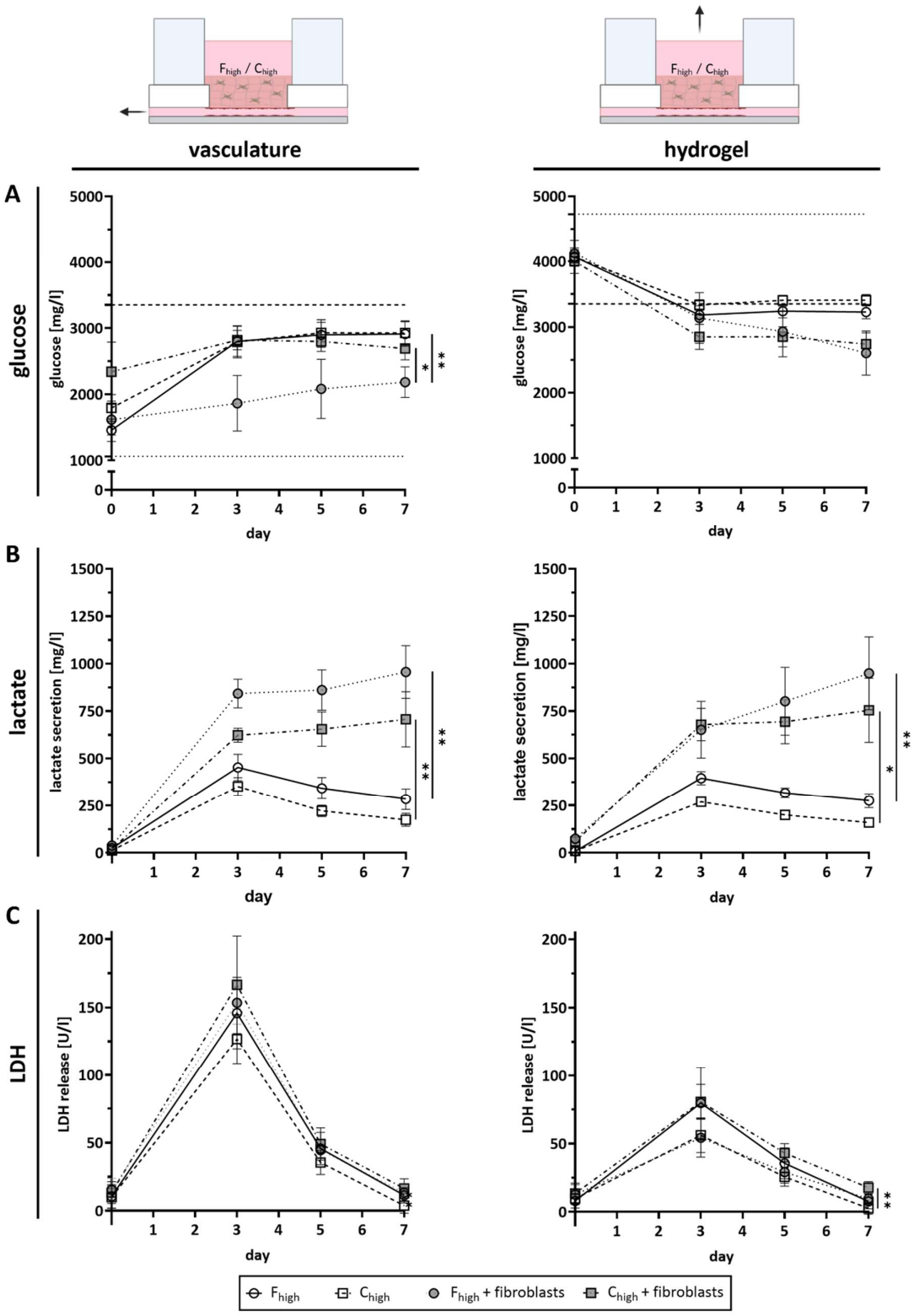

Figure 6: Co-cultures are metabolically stable and viable in the chip over time. Measurement of **(A)** glucose, **(B)** lactate and **(C)** Lactate dehydrogenase (LDH) throughout the 7 day co-culture

period on-chip. Glucose and lactate were used as markers for cell metabolism and LDH as a viability marker. Medium was sampled either from the perfused vasculature or on top of the hydrogel. Whereas ECs were present in all conditions, hydrogels were composed of C_{high} or F_{high} concentrations and with or without fibroblasts. Dotted lines indicate basal glucose levels of respective vasculature and hydrogel medium and dashed lines the basal glucose levels in the whole chip. Shapes represent different conditions as mean ± SEM, $^{**}p \leq 0.01$, $^{*}p \leq 0.05$, tested with one-way ANOVA on day 7. n = 4 independent experiments performed with a minimum of two intra-experimental replicates.

2.7. Inter- and intra- experimental variation

To assess the reproducibility of the methodologies, we additionally determined the inter- and intra-experimental variability for metabolic/viability markers and cytokine secretion at day 7. Between individual experiments (inter-experimental) and within the replicates of a single experiment (intra-experimental), very little variation in glucose and lactate levels was observed in F_{high} and C_{high} cultures when only ECs were present (Supplementary Figure S3). This inter- and intra-experiment variation increased slightly when incorporating fibroblasts into the hydrogel. For LDH release, a similar moderate level of inter- and intra- experimental variation was observed independent of the experimental condition.

When the total cytokine secretion was very low, then the observed inter- and intra-experimental variation was low. This variation increased between different repeats and within individual experiments when increased cytokine secretion was observed (Supplementary Figure S4).

2.8. Monocytes differentiate and migrate across the endothelium into the hydrogel

Finally, to mimic an inflammatory vascular setting more accurately, monocytes were circulated through the vessel and their differentiation into macrophages and migration into the hydrogel was assessed. Blood-derived primary $CD14^{+}$ monocytes were added to the vascular compartment and circulated through the blood vessel for 24 hours before microscopy and flow cytometry analysis (**Figure 7A**). After addition of the monocytes, LDH concentrations slightly

increased for both conditions within the vascular and the hydrogel compartment (**Figure 7B**). However, concentrations were higher in the C_{high} hydrogel, especially within the vasculature (6.3 U/l vs. 15.1 U/l increase). For flow cytometry analysis, single cell suspensions were harvested directly from the circulating vasculature and from the enzymatically digested hydrogel. In comparison to a static control, most of the monocytes on the chip expressed CD68, indicating that they differentiated into a macrophage-like phenotype (**Figure 7C**). This was observed to be independent of the location or hydrogel composition. However, the mean fluorescent intensity (MFI) of CD68 was significantly elevated in F_{high} hydrogels, implying a more pronounced macrophage phenotype (**Figure 7D**). Further characterization revealed that no CD40 was expressed (data not shown), but CD206 across all conditions (**Figure 7E**). Imaging data indicated that the majority of the immune cells attached to the endothelium (**Figure 7F**, i), while a minor proportion migrated deeper into the hydrogel (**Figure 7F**, ii).

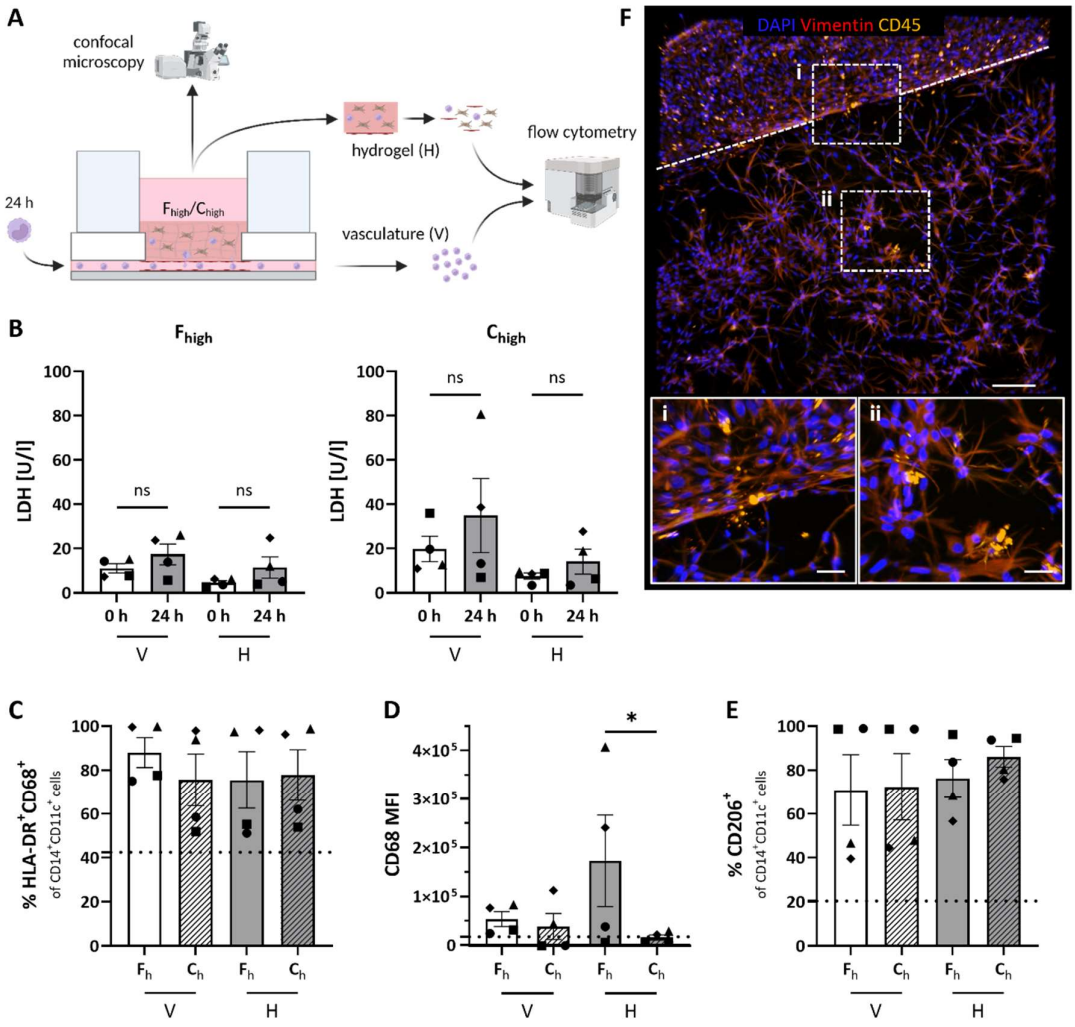

Figure 7: Transendothelial migration and differentiation of monocytes in vessel-on-chip. (A) Monocytes recirculated through the chip vessel for 24 hours. Subsequently, cells were harvested from the vasculature (V) and the hydrogel (H) for flow cytometry analysis. **(B)** LDH analysis in the supernatant of vasculature and hydrogel before addition of the monocytes (0 h) and after 24 h circulation. **(C)** Percentage of HLADR$^+$CD68$^+$ cells within the CD14$^+$CD11c$^+$ cell population. **(D)** MFI of CD68 within the HLADR$^+$CD68$^+$ cells. **(E)** Percentage of CD206 within the CD14$^+$CD11c$^+$ cell population **(F)** Immune cells (CD45, yellow) attach to the vessel walls (i) and migrate into the hydrogel (ii). Vessel-hydrogel interface is indicated by a dotted line. Shown is a representative image of a F_{high} hydrogel as an example. A dotted line represents marker expression of a static control. F_h: high fibrinogen, C_h: high collagen hydrogel concentrations, V: vasculature, H: hydrogel, LDH: lactate dehydrogenase, MFI: mean fluorescent intensity. Scale

bars: 200 µm and 50 µm in magnifications. Shapes represent different donors and columns represent mean ± SEM; n = 4 independent experiments, tested with one-way ANOVA, **$p \leq 0.01$, *$p \leq 0.05$.

3. Discussion

Here, we describe a method to incorporate a vascularized, perfused fibroblast containing connective tissue hydrogel into a MOC and incorporate circulating peripheral blood-derived monocytes. A patterning method was used by printing a water-dissolvable sacrificial structure and connecting a hydrogel channel with the PDMS circulation of the HUMIMIC MOC platform. Thereby, a perfused hydrogel was created. By varying the cell composition and hydrogel component concentrations; C_{high} hydrogel to mimic the healthy situation and F_{high} to mimic early granulation tissue, we demonstrate the versatility of the method. The platform is designed in a manner that facilitates the alteration of the sacrificial hydrogel pattern and the incorporation of different cell types (e.g., immune cells and epithelial cells) and ECM proteins (e.g., elastin, fibronectin, different collagens). This flexibility allows us to specifically address various research questions associated with health and disease.

A commercially available chip system, the HUMIMIC Chip2 24-well was used and combined with a 3D printed sacrificial structure. Perfused vessels can be generated within three days, solely by addition of an ECM and ECs. Flow is generated by a directly integrated micropump consisting of three periodically actuated pumping chambers.[26] Pressure, frequency and direction can be modified. The pulsed flow profile generated in the HUMIMIC Chip2 96-well with empty cell culture compartments has been described earlier.[25] We reproduced the distinct flow profile of one pumping cycle (consisting of four phases) without a hydrogel in the HUMIMIC Chip2 24-well. Notably, after addition of the perfused hydrogel, the flow profile within the hydrogel compartment changed. This steady flow rather than pulsed is most likely caused by the decrease in rigidity and stiffness (elastic modulus) of the softer collagen-fibrinogen hydrogel compared to PDMS which buffers the flow peaks.[27, 28] This results in a constant flow rate and reduced shear stress exerted on the endothelium. We found a decrease for Q_{mean} after addition of the hydrogel. An explanation could be the change in channel geometry and the resulting higher flow resistance. As the pump properties remain unaltered, the mean flow rate decreases

because the addition of a hydrogel increases flow resistance. On rare occasions, detachment of the hydrogel from the hydrogel compartment or the formation of bypasses between the hydrogel and the glass bottom was observed, which can cause turbulence. Therefore, rigorous microscopic quality-control is important throughout the channel formation process. This could be fixed by a coating; however, the presence of the sacrificial structure prohibits liquid coating of the hydrogel compartment after assembly as the structure would be dissolved immediately. Hence, possibilities to anchor the hydrogel to the glass bottom and the compartment walls are limited to pre-coating of individual components before assembly, which complicates the production procedure. Another limitation of our study is the PVA printing resolution, which is currently limited to 400 µm with standard extrusion printers resulting in vessel widths of 500 - 600 µm. Physiologically, this resembles the diameter of small arteries and veins.[29] Even though printing at higher resolutions might be possible, it is very unlikely to generate capillary-like structures below 100 µm with the method described here. Accordingly, alternative techniques such as light-assisted printing or self-assembling of the vascular networks may be required. Compared to the initial sacrificial structure, channel width increased after addition of a hydrogel. This significant increase was more pronounced in F_{high} compared to C_{high} hydrogels. Explanations therefore could be the contraction properties of collagen, higher degradation potential of fibrin under serum-based conditions or the increased secretion of matrix metalloproteinases and higher cellular activity leading to matrix degradation. Supporting this hypothesis, the presence of ECs and fibroblasts may further contribute to this process, as the vessel widening appears to be more pronounced in these conditions.

Glucose, lactate and LDH are standard cell metabolism and viability markers and widely used in the OoC context.[30, 31] By measuring these markers in the medium supernatant of the perfused cultures, we show that the cells were metabolically active and viable throughout 7 days. Most importantly, for all conditions after 3 days, glucose consumption and lactate secretion reached a plateau and LDH release decreased constantly, which indicates stable (co-)culture conditions. As expected, the higher total number of cells resulted in increased glucose consumption and lactate secretion when both ECs and fibroblasts were present. Also, F_{high} hydrogel conditions consumed more glucose and secreted more lactate than C_{high}, indicating that cells in the F_{high} hydrogel have a higher metabolic activity than cells in C_{high} hydrogels. This is in line with the observation of vessel widening, EC sprouting and higher angiogenic cytokine secretion.

Fibrinogen has been shown to increase sprouting of ECs into hydrogels by others as well as us in the past.[32, 33] Furthermore, increased angiogenesis and angiogenic inflammatory cytokine secretion are hallmarks of early granulation tissue formation after wounding which can lead to fibrosis.[34, 35] Therefore, we demonstrate that simple adjustments to the hydrogel composition can impact cellular metabolism and behavior, indicating early granulation tissue.

Of note, for the vasculature compartment, glucose levels were higher in samples than in the medium control used to perfuse the vasculature. This demonstrates that glucose from the higher glucose containing culture medium above the hydrogel diffuses through and mixes with medium in the circulation. This finding is of importance when considering the composition of culture media required to culture organoids in the different compartments within a MOC in the future. It can be assumed that if glucose diffuses through the hydrogel barrier, other components, such as serum and growth factors, will also diffuse through and mix. For day 7, we showed all 72 individual replicates across 4 repeats and 4 biological conditions to illustrate robustness of the (co-)cultures. Between different repeats, variability of glucose and lactate was low without fibroblasts. As expected, intra-experimental variability increased when fibroblasts were added to the hydrogel. Interestingly, glucose concentrations were more suitable to detect abnormal intra-experimental replicates. This is most likely because lactate is produced further downstream in the cell metabolism as it can be derived from pyruvate, the product of glycolysis.[36] For LDH release, inter-experimental variability was slightly higher and could be related to the initial seeding of EC into the microfluidics. The peak in LDH levels is a consequence of non-adherent cells dying and releasing LDH prior their removal upon medium refreshment.

IL-6 and IL-8 are known to be secreted by both cell types, fibroblasts, and ECs.[37, 38] Chronic inflammation often precedes fibrosis, a scarring process with excess ECM secretion because of accumulation, proliferation, and activation of fibroblasts and transition into myofibroblasts.[39, 40] Following up on morphological changes of fibroblast in F_{high} hydrogels which was observed earlier, we measured no differences in IL-6, IL-8 and TNF levels. However, angiogenic cytokine concentration of bFGF, VEGF and sPECAM-1 was increased in the vasculature for F_{high} conditions. Whereas bFGF and VEGF are well characterized angiogenic growth factors, PECAM-1 is more prevalent in its non-soluble form at cell-cell junctions.[41, 42] To our knowledge, soluble PECAM-1 has not been studied in the OoC context. For human umbilical vein endothelial cells,

shedding of PECAM-1 during apoptosis has been described.[43] Although this would suggest increased apoptosis in ECs in F_{high} hydrogels, this hypothesis is not consistent with our measured LDH viability data. Nevertheless, elevated sPECAM-1 levels have also been found in multiple sclerosis patients and are associated with damage of the blood-brain-barrier, thus supporting evidence to use the presented OoC with ECs, F_{high} hydrogel and fibroblasts as a diseased model.[44]

As a first step towards an immune-competent model, we made use of the perfusability of the blood vessel and added monocytes into the circulation. The percentage of HLA-DR$^+$CD68$^+$ cells was higher than the static control across all conditions. However, the MFI of CD68 was higher in F_{high} compared to C_{high} hydrogels. This indicates a high abundance of the receptor and activated macrophages.[45] Supporting the hypothesis of mimicking inflammation onset and early granulation tissue with F_{high} hydrogels, CD68 serves as a valuable histochemical marker for inflamed and tumor tissues.[45] However, the mechanism of macrophages to upregulate CD68 in interaction with fibrinogen remains to be determined. Further characterization of the cells for expression of CD40 (M1) and CD206 (M2) macrophages demonstrated that an M2-like phenotype was acquired on-chip. These macrophages are typically regarded as anti-inflammatory and involved in the processes of wound healing and tissue repair.[46] In adipose tissue, CD206$^+$ tissue resident macrophages have been found to contribute to tissue homeostasis.[47] However, upregulation of this marker in hydrogel and vasculature of both hydrogel conditions suggests either an effect of flow or endocrine signaling from the other cell types leading to this differentiation. Of note, even though an additional washing step was added before digesting the hydrogels for flow cytometry analysis, it is impossible to distinguish between immune cells that have transmigrated into the hydrogel and those that have adhered to the ECs. We therefore also visualized the transmigrated cells in the hydrogel by confocal microscopy.

Under future directions, activation of immune cells could be triggered by the addition of pro-inflammatory cytokines such as TNFα, lipopolysaccharide or heat-killed bacteria. Living bacteria integrated into the model as a microbiome could help unravel host-microbiome interactions and systemic effects across organs. Potential immune-competent organ models and combinations of these include bone marrow, skin, intestine, lymph node, lung, or liver.[48] In addition, the open top design of the chip allows the generation of barrier models (e.g., lung,

gut, skin) on top of a vascularized hydrogel or the incorporation of spheroids directly into the hydrogel. In future studies, the method presented here can be combined with the HUMIMIC Chip4 to connect up to five different vascularized organ models on a single MOC.

4. Conclusions

There is an unprecedented need to create more physiological tissue and organ models, not only in research to understand human (patho-)physiology, but also in toxicology, drug discovery, and in regenerative and personalized medicine. In the past years, tremendous progress has been made in the fields of MPS, 3D (bio-)printing, ECM, and combinations of these just recently, making it possible to increase complexity of organ models by vascularization[49, 50]. However, these models often rely on external tubing and pumps to generate perfusion and require complex experimental setups, making them extremely difficult to reproduce.

Our study presents an extremely versatile and easy method to generate vascularized perfused hydrogels in a MOC platform. Stable blood vessels can be generated within three days and hydrogel concentrations can be modified to generate a healthy or diseased vessel. Perfusion with monocytes shows they differentiate into macrophages and can transmigrate across the endothelium and enter the hydrogel. This makes it an extremely valuable tool to engineer the next generation of vascularized and immune-competent organ models in the future.

5. Methods

Cell culture: Human skin from healthy donors was collected as surgical waste after abdominal dermolipectomy. The tissue was used in an anonymous fashion and all donors gave informed consent as described in the 'Code of Conduct for Health Research' as formulated by COREON (Committee on Regulation of Health Research; https://www.coreon.org) and the following procedures were approved by the institutional review board of the Amsterdam UMC.

Fibroblasts and endothelial cells: Dermal fibroblasts were isolated from human skin as described earlier.[51] Cells were cultured in fibroblast medium consisting of Dulbecco's modified Eagle's medium (DMEM; Thermo Fisher Scientific, Waltham, MA, USA), supplemented with 1% UltroserG (BioSepra, Cergy, France) and 1% penicillin/streptomycin (P/S; Invitrogen, Paisley, UK). Cells were cultured at 37 °C, 5% CO_2, medium was exchanged every 3-4 days and cells were used at passage ≤ 3. Dermal endothelial cells (ECs) were isolated from human dermis. After enzymatic digestion of the dermal fraction of the skin, cells were cultured in Endothelial Cell Growth Medium MV2 (MV2; PromoCell, Heidelberg, Germany), always supplemented with 1% P/S. When endothelial colonies were formed, the endothelial population was enriched with a CD31 MicroBead Kit (Miltenyi Biotec, Bergisch Gladbach, Germany). Cells were amplified in MV2 and after harvesting, ECs were labeled with anti-human podoplanin Alexa-488 and anti-human CD31 PE (both BioLegend, San Diego, CA, USA) and subsequently sorted on a BD FACSAria™ Fusion Flow Cytometer (BD Biosciences, Franklin Lakes, NJ, USA) into a pure population of $CD31^{+}PDPN^{-}$ blood endothelial cells (BECs). Cells were cultured at 37 °C, 5% CO_2 in MV2 and medium was exchanged every 3-4 days. Cells at passage ≤ 8 were used for experiments.

Peripheral blood derived monocytes: Human monocytes were isolated using magnetic-activated cell sorting with $CD14^{+}$ magnetic beads from peripheral blood mononuclear cells (PBMCs) as previously described.[52] At day 3, monocytes were added to the MOC for 24 hours at 3.5×10^5 cells per chip in media composed of RPMI-1640 (Lonza, Basel, Switzerland) supplemented with 10% fetal calf serum (FCS; GE Healthcare, Chicago, IL, USA), 50 µM β-mercaptoethanol (Merck, Darmstadt, Germany), 100 IU/ml sodium-penicillin (Thermo Fisher Scientific), 100 µg/ml streptomycin (Thermo Fisher Scientific), and 2 mM L-glutamine (Thermo Fisher Scientific).

Microphysiological system (multi-organ-chip): A modified version of the HUMIMIC Chip2 24-well (TissUse) was used with a sacrificial print. The computer aided design (CAD) model to generate the PVA structure was created in solidworks (v2018; Dassault Systèmes SOLIDWORKS, Waltham, MA, USA) and printed with an Ultimaker S5 (Ultimaker, Utrecht, The Netherlands); BB printcore and a 0.4 mm nozzle, according to the manufacturer's instructions. Recirculating Flow was applied with a HUMUMIC Starter (TissUse) control unit at 30 bpm, ± 500 mbar, counterclockwise.

Hydrogels: Two different hydrogels containing differing ratios of collagen and fibrinogen were used in experiments, based on previous publications.[53, 54] Collagen was isolated from rat tails and dissolved in 0.1% acetic acid (VWR, Radnor, PA). Then, 10x HBSS (Thermo Fisher Scientific) was added to the collagen solution (diluted 1:8) and the pH neutralized with 1M NaOH. High collagen (C_{high}) hydrogels were composed of a final concentration of 3 mg/ml collagen and 1 mg/ml fibrinogen (Diagnostica Stago, Paris, France). For high fibrinogen (F_{high}) conditions, hydrogels were composed of a final concentration of 2.5 mg/ml fibrinogen and 0.1 mg/ml collagen. To the collagen/fibrinogen mixture of both hydrogel conditions, final concentrations of 50 KIU/ml aprotinin (SERVA, Heidelberg, Germany) and 0.5 U/ml thrombin (Merck) were added and resuspended thoroughly before casting. After plasma activation, 350 µl hydrogel with or without 7 x 10^4 fibroblasts/ml was casted into the hydrogel compartment of the chip, covering the sacrificial PVA structure. Chips with hydrogels were subsequently incubated at 37 °C for 30 min for collagen-fibrin network formation and polymerization. Next, 300 µl MV2 was added to the vascular compartment and 500 µl fibroblast medium to the hydrogel compartment and the chip was connected to the HUMIMIC Starter to apply flow, then incubated overnight at 37 °C, 5% CO_2.

Blood endothelial cell seeding: To flush out residual printed sacrificial structures, the vascular compartment was washed with 300 µl MV2 before seeding the cells. Then, 5 x 10^5 BECs were seeded into the patterned hydrogel structure via the pressure differences after adding the cell suspension to the vascular compartment. Chips were subsequently incubated at 37 °C, 5% CO_2 for 4 hours. After 4 hours, the vascular compartment was washed with 300 µl MV2. Then, 300 µl fresh MV2 was added to the vascular compartment and 500 µl fibroblast medium on top of the hydrogel, both media supplemented with 50 KIU/ml aprotinin. MV2 and fibroblast medium were always supplemented with 50 KIU/ml aprotinin from here on. A full medium exchange

was performed on day 3 and day 5 for both compartments: in the vascular compartment 300 µl MV2 was collected and replaced with fresh medium and for the hydrogel compartment, 500 µl fibroblast medium was collected and replaced with fresh medium. On day 7, media from the different compartments was collected. For all time points, media was stored separately at 4 °C until metabolic analysis was performed. Afterwards, the media was stored at -20 °C until further analysis.

Fluid dynamics characterization - flow rates and shear stress: To characterize the flow dynamics, the flow velocity within the channels was measured with time and spatial resolution using micro-particle image velocimetry (µPIV). The measurement method was described previously in literature.[55] First, chips were filled with 0.4% w/v 5 µm Aldehyde/Sulfate Latex Beads in PBS (Thermo Fisher Scientific) as tracer particles and 0.1% Triton-X-100 (VWR) to reduce the sedimentation. The chips were then connected to a pneumatic control unit (TissUse) and perfused with a frequency of 30 bpm, and pressure/vacuum of ± 500 mbar. The µPIV measurements were performed using an inverted microscope Axio Vert.A1 (Zeiss, Jena, Germany) with a 2.5x objective, LED light source and a high-speed camera HXC40 (Baumer, Friedberg, Germany). For the measurement, the center of the channel was focused to capture the maximum velocity of the particles. The recorded image series were analyzed with the open-source toolbox PIVLab for MATLAB for mean flow velocity and its extrema.[56]

Based on the measured velocity, the mean wall shear stress (WSS_{mean}) was determined for a rectangular channel according to Hagen-Poiseuille's law from the dynamic viscosity η of the medium, the mean flow velocity Q and the width w and height h of the channel (adapted from [57]):

$$WSS_{\text{mean}} = \frac{6\eta Q}{h^3 + h^2 w}\left[1 - \sum_{i=2a+1}^{\infty} \frac{1}{i^5}\frac{192}{\pi^5}\frac{h}{w}\tanh\left(i\pi\frac{w}{2h}\right)\right]^{-1}, (a\epsilon\mathbb{N})$$

As it was not possible to determine the wall shear stress for channels with complex cross-sectional geometries analytically, the WSS for the hydrogel channel was determined with a simulation. For this purpose, the cross-sectional geometry of the channels was measured with a Nikon AX R confocal microscope (Nikon, Tokyo, Japan) and modulated three-dimensionally as a straight channel. A laminar flow was assumed for the simulation and the mean velocity of the fluid previously measured by µPIV was used as a boundary condition.

Immunofluorescent staining: All flow incubations conducted in this section were performed with the following perfusion settings: 30 bpm, ± 500 mbar, counterclockwise. Hydrogels were preserved in chips directly by adding 4% paraformaldehyde (Electron Microscopy Sciences, Hatfield, PA, USA), followed by incubation for 10 min in flow and 1 hour static at RT. Chips were then pre-treated with 0.2% Triton in PBS, 10 minutes in flow at RT before the immunostaining. Next, chips (100 µl to the vascular and 200 µm to the hydrogel compartment on top of the hydrogel) were incubated with mouse anti-human CD31 (Dako, Glostrup, Denmark), incubated for 30 minutes in flow at RT and afterwards overnight static at 4 °C. The following day, chips were washed twice with 0.2% Triton in PBS and then incubated with goat anti-mouse 488 (Thermo Fisher Scientific), directly labeled anti-vimentin Alexa Fluor 647 (BioLegend) and DAPI (Invitrogen) for 30 minutes in flow at RT followed by an overnight static incubation at 4 °C. The following day, chips were washed twice with 0.2% Triton in PBS and stored at 4 °C until analysis.

FITC-dextran permeation analysis: FITC-dextran (70 kDA; Sigma-Aldrich, St. Louis, MO, USA) was dissolved in PBS and used in a final concentration of 0.5 mg/ml. 100 µl were added to the vascular compartment of the MOC and images were taken after a 10 minute perfusion.

Microscopy and channel width measurements: Bright field images and FITC-dextran perfusion images were taken with a Keyence BZ-X700E (Keyence, Osaka, Japan) and analyzed in the BZ-X800 Analyzer (v1.1.2; Keyence). Channel widths were measured in bright field, perpendicular to the channels in triplicates for ≥ 11 individual circulations per condition, either 24 hours after the gel was cast (+/-/-) or with cells at day 7 (+/+/- and +/+/+) (Supplementary Figure S2A). Fluorescent images were taken with a Nikon ECLIPSE Ti2 (Nikon, Tokyo, Japan) and confocal images with a Nikon AX R (Nikon). Images were analyzed in Imaris (v10.1.0; Oxford Instruments, Oxfordshire, UK). As quality control, all hydrogels were imaged on day 7 (Supplementary Figure S2B).

Viability and metabolic analysis: To measure levels of glucose, lactate as well as lactate dehydrogenase (LDH) activity, medium was analyzed on day 0 (before addition of ECs), 3, 5 and 7, with an Indiko™ Plus Clinical Chemistry Analyzer (Thermo Fisher Scientific) in combination with the Glucose (HK) 981779 kit (Thermo Fisher Scientific), Lactate Fluitest LA 3011 kit (Analyticon Biotechnologies, Lichtenfels, Germany), and LDH IFCC 981782 kit (Thermo Fisher Scientific), as well as the Cytotoxicity Detection Kit PLUS (LDH) (for Figure 7; Roche, Basel, Switzerland), according to the manufacturer's instructions. MV2 and fibroblast medium were

used as controls and basal glucose levels in the whole circulation calculated with the ratio of 3/8 vasculature and 5/8 hydrogel medium.

Cytokine analysis: The Human Angiogenesis Panel V02 (BioLegend, San Diego, CA, USA) cytokine bead array was used to measure concentrations of Interleukin-6 (IL-6), IL-8, tumor necrosis factor α (TNFα), basic fibroblast growth factor (bFGF), vascular endothelial growth factor (VEGF), soluble platelet endothelial cell adhesion molecule (sPECAM-1), epidermal growth factor (EGF), phosphatidylinositol-glycan biosynthesis class F (PIGF), Angiopoeitin-1 and Angiopoeitin-2. The assay was performed according to the manufacturer's instructions and acquired on an Attune NxT flow cytometer (Thermo Fisher Scientific). Data was analyzed with the LEGENDplex Data Analysis Software Suite (BioLegend).

Multispectral flow cytometry: Cells were added to the vascular compartment on day 3 and circulated on the chip for 24 hours (Supplementary Figure S5A). Then, cells were collected from the vasculature compartment. The vasculature compartment was washed with fresh medium by pumping at RT for 10 min to remove remaining cells which did not attach. Hydrogels were subsequently enzymatically digested into a single cell suspension for flow cytometry. Hydrogels were incubated in 0.2 mg/ml Collagenase P and 0.1 mg/ml DNase I (both from Sigma-Aldrich) for 1 h at 37 °C. Afterwards, the reaction was stopped with 2% FCS and 5 mM EDTA (Sigma-Aldrich) in PBS.

Cell suspensions were stained in a 96-well plate at 4 °C for multispectral flow cytometry analysis. Cells were first washed with PBS and stained with a fixable viability dye in 1:2000 (eFluor™ 780 labeled; Invitrogen) for 10 minutes at 4 °C. Next, cells were washed with 0.1% BSA and 0.05% NaN_3 in PBS (FACS buffer) prior to Fc-receptor blocking with 10% normal human serum in FACS buffer. Cells were then incubated with directly-labeled antibodies, against extracellular markers, diluted in blocking buffer in the following dilutions: anti-CD11c in 1:200 (BUV661 labeled), anti-CD14 in 1:50 (pacific blue labeled), anti-HLA-DR in 1:100 (BV711 labeled), anti-CD206 in 1:50 (FITC labeled) and anti-CD40 in 1:50 (APC labeled; all BioLegend). After staining, cells were washed two times with FACS buffer and fixed with 2% PFA (VWR) for 10 minutes at RT. Cells were then washed with 0.5% Saponin buffer, and the intracellular antibody was added, anti-CD68 in 1:100 (BV785 labeled; BioLegend). Samples and single stains on beads were acquired on Aurora 5-laser Flow Cytometer (Cytek; Fremont, CA, USA). Data was analyzed with FlowJo (v10.7; Ashland, OR, USA) and OMIQ (Boston, MA, USA). Analysis of

monocytes and macrophages was based on a gating strategy to exclude other cell types such as ECs and fibroblasts (Supplementary Figure S5B). Monocytes were gated on cells, single cells, live cells, $CD14^{+}CD11c^{+}HLADR^{+}CD68^{-}$ and macrophages on $CD14^{+}CD11c^{+}HLADR^{+}CD68^{+}$ (Supplementary Figure S5C).

Statistical analysis: Data is presented as mean ± standard error of the mean. The number of different skin donors and the number of independent experiments is described in the legends of each figure. GraphPad Prism (v9.5.1; GraphPad Software Inc., La Jolla, CA, USA) was used for statistical analysis with tests indicated in figure legends. Differences were considered as significant when $p \leq 0.05$.

Author Contributions

Conceptualization: JJ, ED, SG; Funding Acquisition: ED, SG; Investigation: JJ, AIM, HE, MT; Methodology: JJ, PB, AIM, ED, SG, JJK; Project administration: ED, SG, JJK; Visualization: JJ, HE; Writing-Original Draft Preparation: JJ, SG, JJK; Writing-Review and Editing: JJ, AIM, HE, ED, SG, JJK.

Conflict of Interest

PB, HE and ED employed by TissUse GmbH, Berlin, Germany. The remaining authors declare that the research was conducted in the absence of any commercial or financial relationships that could be construed as a potential conflict of interest.

Acknowledgments

The presented work was funded by the SMART Organ-on-Chip consortium, NWO-TTW Perspective Programme of the Dutch Research Council (NWO; project no. P19-03), the European Union's Horizon 2020 research and innovation program (grant agreement no. 847551) ARCAID, the LymphChip consortium, NWA-ORC programme of the Dutch Research Council (NWO; project no. 1292.19.019) the ReSHAPE consortium, EU-H2020 (grant agreement no. 825392), and the BIRDIE consortium, EU-H2020 (grant agreement no. 964452). Views and opinions expressed are however those of the author(s) only and do not necessarily reflect those of the European Union or the European Health and Digital Executive Agency (HADEA). Neither the European Union nor the granting authority can be held responsible for them. The authors would like to thank Artur Christian Garcia da Silva for the FITC-dextran permeation assay and the Microscopy & Cytometry Core Facility at Amsterdam UMC (location Vrije Universiteit Amsterdam) for their support.

References

1. Frantz, C., Stewart, K.M. & Weaver, V.M. The extracellular matrix at a glance. *J Cell Sci* **123**, 4195-4200 (2010).
2. Pugsley, M.K. & Tabrizchi, R. The vascular system: An overview of structure and function. *Journal of Pharmacological and Toxicological Methods* **44**, 333-340 (2000).
3. Picollet-D'hahan, N., Zuchowska, A., Lemeunier, I. & Le Gac, S. Multiorgan-on-a-Chip: A Systemic Approach To Model and Decipher Inter-Organ Communication. *Trends in Biotechnology* **39**, 788-810 (2021).
4. Dejana, E. Endothelial cell–cell junctions: happy together. *Nature Reviews Molecular Cell Biology* **5**, 261-270 (2004).
5. Nourshargh, S. & Alon, R. Leukocyte Migration into Inflamed Tissues. *Immunity* **41**, 694-707 (2014).
6. Adams, R.H. & Alitalo, K. Molecular regulation of angiogenesis and lymphangiogenesis. *Nature Reviews Molecular Cell Biology* **8**, 464-478 (2007).
7. Waasdorp, M. et al. in Biomolecules, Vol. 11 (2021).
8. Jensen, C. & Teng, Y. Is It Time to Start Transitioning From 2D to 3D Cell Culture? *Frontiers in Molecular Biosciences* **7** (2020).
9. Marx, U. et al. Biology-inspired microphysiological systems to advance patient benefit and animal welfare in drug development. *ALTEX - Alternatives to animal experimentation* **37**, 365-394 (2020).
10. Bhatia, S.N. & Ingber, D.E. Microfluidic organs-on-chips. *Nature Biotechnology* **32**, 760-772 (2014).
11. Ingber, D.E. Human organs-on-chips for disease modelling, drug development and personalized medicine. *Nature Reviews Genetics* **23**, 467-491 (2022).
12. Aazmi, A. et al. Engineered Vasculature for Organ-on-a-Chip Systems. *Engineering* **9**, 131-147 (2022).
13. Shirure, V.S., Hughes, C.C.W. & George, S.C. Engineering Vascularized Organoid-on-a-Chip Models. *Annual Review of Biomedical Engineering* **23**, 141-167 (2021).
14. Massa, S. et al. Bioprinted 3D vascularized tissue model for drug toxicity analysis. *Biomicrofluidics* **11**, 044109 (2017).
15. Lin, N.Y.C. et al. Renal reabsorption in 3D vascularized proximal tubule models. *Proceedings of the National Academy of Sciences* **116**, 5399-5404 (2019).
16. Zheng, Y. et al. In vitro microvessels for the study of angiogenesis and thrombosis. *Proceedings of the National Academy of Sciences* **109**, 9342-9347 (2012).
17. Schöneberg, J. et al. Engineering biofunctional in vitro vessel models using a multilayer bioprinting technique. *Scientific Reports* **8**, 10430 (2018).
18. Paek, J. et al. Microphysiological Engineering of Self-Assembled and Perfusable Microvascular Beds for the Production of Vascularized Three-Dimensional Human Microtissues. *ACS Nano* **13**, 7627-7643 (2019).
19. Campisi, M. et al. 3D self-organized microvascular model of the human blood-brain barrier with endothelial cells, pericytes and astrocytes. *Biomaterials* **180**, 117-129 (2018).
20. Wufuer, M. et al. Skin-on-a-chip model simulating inflammation, edema and drug-based treatment. *Scientific Reports* **6**, 37471 (2016).
21. Maurer, M. et al. A three-dimensional immunocompetent intestine-on-chip model as in vitro platform for functional and microbial interaction studies. *Biomaterials* **220**, 119396 (2019).
22. Huh, D. et al. Reconstituting Organ-Level Lung Functions on a Chip. *Science* **328**, 1662-1668 (2010).
23. Li, J., Chen, J. & Kirsner, R. Pathophysiology of acute wound healing. *Clinics in Dermatology* **25**, 9-18 (2007).
24. Ataç, B. et al. Skin and hair on-a-chip: in vitro skin models versus ex vivo tissue maintenance with dynamic perfusion. *Lab on a Chip* **13**, 3555-3561 (2013).

25. Schimek, K. et al. Integrating biological vasculature into a multi-organ-chip microsystem. *Lab on a Chip* **13**, 3588-3598 (2013).
26. Wu, M.-H., Huang, S.-B., Cui, Z., Cui, Z. & Lee, G.-B. A high throughput perfusion-based microbioreactor platform integrated with pneumatic micropumps for three-dimensional cell culture. *Biomedical Microdevices* **10**, 309-319 (2008).
27. Izdihar, K. et al. in Applied Sciences, Vol. 11 (2021).
28. Dutov, P., Antipova, O., Varma, S., Orgel, J.P.R.O. & Schieber, J.D. Measurement of Elastic Modulus of Collagen Type I Single Fiber. *PLOS ONE* **11**, e0145711 (2016).
29. Camasão, D.B. & Mantovani, D. The mechanical characterization of blood vessels and their substitutes in the continuous quest for physiological-relevant performances. A critical review. *Materials Today Bio* **10**, 100106 (2021).
30. Bauer, S. et al. Functional coupling of human pancreatic islets and liver spheroids on-a-chip: Towards a novel human ex vivo type 2 diabetes model. *Scientific Reports* **7**, 14620 (2017).
31. Tantengco, O.A.G. et al. Modeling ascending Ureaplasma parvum infection through the female reproductive tract using vagina-cervix-decidua-organ-on-a-chip and feto-maternal interface-organ-on-a-chip. *The FASEB Journal* **36**, e22551 (2022).
32. van Hinsbergh, V.W.M., Collen, A. & Koolwijk, P. Role of Fibrin Matrix in Angiogenesis. *Annals of the New York Academy of Sciences* **936**, 426-437 (2001).
33. Monsuur, H.N., Weijers, E.M., Gibbs, S. & van den Broek, L.J. Skin substitutes are more potent than dermal or epidermal substitutes in stimulating endothelial cell sprouting. *BMC Biomedical Engineering* **1**, 18 (2019).
34. Greaves, N.S., Ashcroft, K.J., Baguneid, M. & Bayat, A. Current understanding of molecular and cellular mechanisms in fibroplasia and angiogenesis during acute wound healing. *Journal of Dermatological Science* **72**, 206-217 (2013).
35. Li, J., Zhang, Y.-P. & Kirsner, R.S. Angiogenesis in wound repair: Angiogenic growth factors and the extracellular matrix. *Microscopy Research and Technique* **60**, 107-114 (2003).
36. Greene, M. in Encyclopedia of Cancer. (ed. M. Schwab) 1917-1922 (Springer Berlin Heidelberg, Berlin, Heidelberg; 2017).
37. Akira, S., Taga, T. & Kishimoto, T. in Advances in Immunology, Vol. 54. (ed. F.J. Dixon) 1-78 (Academic Press, 1993).
38. Baggiolini, M., Loetscher, P. & Moser, B. Interleukin-8 and the chemokine family. *International Journal of Immunopharmacology* **17**, 103-108 (1995).
39. Van Linthout, S., Miteva, K. & Tschöpe, C. Crosstalk between fibroblasts and inflammatory cells. *Cardiovascular Research* **102**, 258-269 (2014).
40. Wynn, T.A. & Ramalingam, T.R. Mechanisms of fibrosis: therapeutic translation for fibrotic disease. *Nature Medicine* **18**, 1028-1040 (2012).
41. Cross, M.J. & Claesson-Welsh, L. FGF and VEGF function in angiogenesis: signalling pathways, biological responses and therapeutic inhibition. *Trends in Pharmacological Sciences* **22**, 201-207 (2001).
42. Woodfin, A., Voisin, M.-B. & Nourshargh, S. PECAM-1: A Multi-Functional Molecule in Inflammation and Vascular Biology. *Arteriosclerosis, Thrombosis, and Vascular Biology* **27**, 2514-2523 (2007).
43. Ilan, N., Mohsenin, A., Cheung, L. & Madri, J.A. PECAM-1 shedding during apoptosis generates a membrane-anchored truncated molecule with unique signaling characteristics. *The FASEB Journal* **15**, 362-372 (2001).
44. Kalinowska, A. & Losy, J. PECAM-1, a key player in neuroinflammation. *European Journal of Neurology* **13**, 1284-1290 (2006).
45. Chistiakov, D.A., Killingsworth, M.C., Myasoedova, V.A., Orekhov, A.N. & Bobryshev, Y.V. CD68/macrosialin: not just a histochemical marker. *Laboratory Investigation* **97**, 4-13 (2017).
46. Rőszer, T. Understanding the Mysterious M2 Macrophage through Activation Markers and Effector Mechanisms. *Mediators of Inflammation* **2015**, 816460 (2015).

47. Nawaz, A. et al. CD206+ M2-like macrophages regulate systemic glucose metabolism by inhibiting proliferation of adipocyte progenitors. *Nature Communications* **8**, 286 (2017).
48. Morrison, A.I., Sjoerds, M.J., Vonk, L.A., Gibbs, S. & Koning, J.J. In vitro immunity: an overview of immunocompetent organ-on-chip models. *Frontiers in Immunology* **15** (2024).
49. Sun, S., Jin, L., Zheng, Y. & Zhu, J. Modeling human HSV infection via a vascularized immune-competent skin-on-chip platform. *Nature Communications* **13**, 5481 (2022).
50. Grigoryan, B. et al. Multivascular networks and functional intravascular topologies within biocompatible hydrogels. *Science* **364**, 458-464 (2019).
51. Kroeze, K.L. et al. Chemokine-Mediated Migration of Skin-Derived Stem Cells: Predominant Role for CCL5/RANTES. *Journal of Investigative Dermatology* **129**, 1569-1581 (2009).
52. Morrison, A.I. et al. An Organotypic Human Lymph Node Model Reveals the Importance of Fibroblastic Reticular Cells for Dendritic Cell Function. *Tissue Engineering and Regenerative Medicine* **21**, 455-471 (2024).
53. Kim, S., Lee, H., Chung, M. & Jeon, N.L. Engineering of functional, perfusable 3D microvascular networks on a chip. *Lab on a Chip* **13**, 1489-1500 (2013).
54. Jäger, J. et al. Reconstructed Human Skin with Hypodermis Shows Essential Role of Adipose Tissue in Skin Metabolism. *Tissue Engineering and Regenerative Medicine* (2024).
55. Lindken, R., Rossi, M., Große, S. & Westerweel, J. Micro-Particle Image Velocimetry (µPIV): Recent developments, applications, and guidelines. *Lab on a Chip* **9**, 2551-2567 (2009).
56. Thielicke, W. & Stamhuis, E.J. PIVlab – Towards User-friendly, Affordable and Accurate Digital Particle Image Velocimetry in MATLAB. *Journal of Open Research Software* (2014).
57. Bruus, H. Theoretical Microfluidics. (2008).

Supplementary Information

A Sacrificial 3D Printed Vessel-on-Chip Demonstrates a Versatile Approach to Model Connective Tissue Pathology

*Jonas Jäger, Phil Berger, Andrew I. Morrison, Hendrik Erfurth, Maria Thon, Eva-Maria Dehne, Susan Gibbs, and Jasper J. Koning**

*correspondence: jj.koning@amsterdamumc.nl

Figure S1: Study setup in figures, experimental timeline and fit of the PVA structure. Addition to Figure 1. **(A)** Experimental setup of the study, shown in Figures. **(B)** Chips were produced and hydrogel (+/- fibroblasts) and ECs added. Subsequently, the vessels were perfused for 7 days. ECs: endothelial cells, ME: medium exchange, LDH: lactate dehydrogenase, F_{high}: high fibrinogen, C_{high}: high collagen hydrogel concentrations. **(C)** Bright-field image of the PVA-PDMS interface shows fit of the sacrificial structure in the PDMS channel. Scale bar: 1000 µm.

Figure S2: Vessel width measurements and hydrogel shrinkage quality control. Addition to Figure 4C. **(A)** Addition of a hydrogel on top of the sacrificial structure induced widening of the channel. Images were taken before the addition of the hydrogel and after 24 hours. Red lines indicate channel alignment and perpendicular width measurement. Scale bars: 1000 µm in overview, 500 µm in magnifications. **(B)** Gross bright-field images of F_{high} and C_{high} hydrogels in chip with ECs and fibroblasts at day 7. Shown are representative images for 3 different replicates. Scale bars: 2000 µm.

Figure S3: Metabolic markers of EC-fibroblast co-cultures show low variability between different repeats. Individual repeats of Figure 6. Variability between different repeats and inter-experimental variability of a total of N = 72 (≙ 36 chips) individual measurements at day 7. For vasculature and hydrogel measurements of glucose, lactate and LDH, four conditions are shown with intra-experimental replicates (each column) and repeats (1-4). Dotted lines indicate basal glucose levels of respective vasculature and hydrogel medium and dashed lines the basal glucose levels in the whole chip. Shapes represent different conditions and line mean of intra-experimental replicates.

Figure S4: Variability of cytokine secretion. Individual repeats of Figure 5. Measurement of 10 different cytokines shows variability between different repeats and inter-experimental variability of a total of N = 72 (≙ 36 chips). Shown are individual measurements on day 7.

Figure S5: Experimental timeline and gating strategy for monocytes and macrophages. Addition to Figure 7. **(A)** Experimental timeline for 24 h monocyte perfusion on-chip. **(B)** Monocytes were directly gated based on size and granularity (FSC-SSC) to initially remove other cell types such as fibroblasts and ECs together with debris. Hydrogel and vasculature samples of the same circulation are shown as an example. **(C)** Gating was set on cells, single cells, live cells, $CD14^{+}CD11c^{+}$ cells, $HLADR^{+}CD68^{+}$ and $CD40^{+}$ or $CD206^{+}$ for M1 and M2 macrophages. FSC: forwards scatter, SSC: side scatter.

Movie S1: Hydrogel channel rendering. ECs were stained with vimentin (yellow) and nuclei with DAPI (blue). Surface-rendering is shown in red.